ELSEVIER

Cement and Concrete Composites **19** (1997) 59–68

0958-9465/97/$17.00 + 0.00

PII:S0958-9465(96)00041-8

Fiber-optic Crack-tip Opening Displacement Sensor for Concrete

Insang Lee, Yuan Libo, Farhad Ansari* & Hong Ding

Smart Sensors & NDT Laboratory, Department of Civil and Environmental Engineering, New Jersey Institute of Technology, Newark, NJ 07102, USA

Abstract

The development of a fiber-optic sensor for embedment in cementitious composites and measurement of displacements associated with the opening of microcracks are described. The sensor can be employed as a transducer for measurement of crack-tip opening displacements during fracture tests. A polarization-maintaining optical fiber is used as the sensing element, and the transduction mechanism is similar to those of other sensors based on polarimetric-type based fibers. However, the deformation resolving power of the sensor is increased by way of increasing the effective length of the optical fiber. This is done by winding the optical fiber into a coil. A direct relationship between the number of loops in the coil and sensitivity of measurements is obtained. A calibration procedure is developed by which the optical signal is converted to displacements. The sensor was employed in a series of fracture tests. Experiments involved embedment of the optical fiber in concrete beams. Specimens were center-edge-notched, and the fiber coil sensors were embedded at the tip of the notch. This arrangement allowed for direct measurement of displacements associated with the opening of microcracks at the crack tip. Experimental results are presented, and crack-tip opening displacement (CTOD) results are compared with crack-opening displacements measured by conventional transducers at the crack mouth (COD). © 1997 Elsevier Science Limited

Keywords: Cracking, microcracks, concrete, crack-tip opening displacement, crack-opening displacement, process zone, fiber-optic sensors, polarimetric sensors, embedded sensors.

*To whom correspondence should be addressed.

INTRODUCTION

Cracking is among the important parameters that directly influence the structural design and durability of construction. Many fracture-mechanics models have been proposed in recent years to account for the non-linear behavior of concrete elements.[1] Non-linear characteristics of fracture in concrete are associated with the microcracking zone (process zone) in front of the crack tip.[2] Most fracture models represent the fracture process zone by a damage band or a band of crack-closing pressure which depends on the crack-opening displacement, i.e. the post-peak stress–displacement relationship. The accuracy of these models relies significantly on the post-peak stress–displacement relationship selected. One parameter of significant importance in determining fracture properties is crack-tip opening displacement (CTOD). For instance, crack extension or fracture may be assumed to occur when the crack-opening displacement exceeds a critical value. To date, experimental determination of CTOD has been an impossibility. For these reasons researchers have resorted to measurement of crack-mouth opening displacement (COD) on a notched or precracked specimen by linear variable displacement transducers (LVDT) or clip-gage extensometers. It is logical to assume that the crack-mouth opening displacements measured in this way should be larger than the real displacements at the crack tip. This is due to the fact that in comparison with CTOD, COD represents displacements at distances further away from the neutral axis of the beam. Furthermore, COD values are more representative of global displacements rather than deformations specific to the formation of a process zone

in cementitious composites. For these reasons, attempts have been made to determine CTOD from measurement of surface deformations using laser speckle interferometry.[3] These studies indicated the localized nature of microcracking at the crack tip, and the need for characterization of displacements in terms of the opening of microcracks within the process zone. Therefore, there is a need to develop a very sensitive sensor for embedment at the crack tip and within the microcracking zone.

The objective of the research presented here is to develop, calibrate and test an embedded optical-fiber CTOD sensor for applications in fracture mechanics studies of cementitious composites. Among the important characteristics of optical fibers are small size, geometric adaptability, and the ability to act as the sensor as well as the signal path. These are important attributes, especially in consideration of the design of practicable embedded sensors in concrete and other cementitious composites. In general, fiber-optic sensors are categorized into various types depending on the application and transduction mechanism employed for discernment of material deformations. Detailed discussion pertaining to various types of fiber-optic sensor and arrangements for the measurement of deformations is beyond the scope of this paper. However, it is important to note that a suitable CTOD sensor for concrete requires sufficient sensitivity for measurement of deformations, economy in terms of sensor complexity, instrumentation and practicality, and ease of installation during placement of fresh concrete. The sensor described herein was designed based on these considerations. A calibration technique is developed for conversion of optical signals to corresponding displacements. The capability of the fiber-optic sensor in terms of sensitivity and resolution power for measurement of CTOD is demonstrated through experiments with single-edge-notched concrete beams under three-point bending conditions.

SENSING METHODOLOGY

The sensor developed herein employs a high birefringent (Hi-Bi) optical fiber for sensing of strains and deformations. Hi-Bi fibers possess properties similar to those of birefringent materials employed in photoelasticity.[4] These fibers divide the circularly polarized light entering them into two modes along the two orthogonal axes (principal axes) of the optical fiber. Light waves exiting the output of the fiber will also be circularly polarized (Fig. 1). The intensity of light at the output end of the fiber is of the form:[5,6]

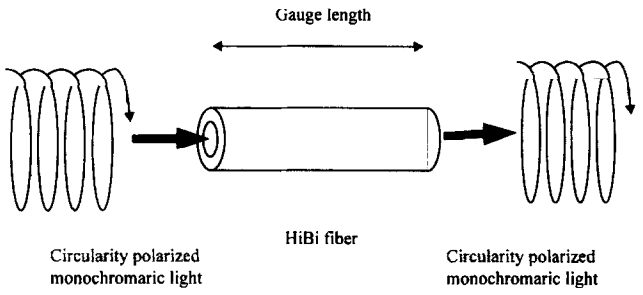

Fig. 1. Basic principle for a polarimetric sensor.

$$I = \frac{1}{2}(1+\cos\phi) \tag{1}$$

where I is the intensity of light and ϕ is the relative phase retardation, which will be shown to be related to the fiber length and the optical properties of the fiber. In the absence of strains and/or other perturbations, the exiting light will have a constant output. External perturbations such as deformations along the length of the optical fiber will cause interference between the two modes, resulting in a change in the relative phase retardation by the amount $\Delta\phi$. The output intensity will have a sinusoidal shape and, in the time domain, the period of this sinusoidal waveform is termed a fringe. The frequency of the fringe pattern depends on the magnitude of the applied strain, and allows for development of a strain or deformation sensor through calibration. The relative phase retardation ϕ is related to the propagation constant, β, and the original length of the fiber, l_o (gage length), through the following relationship:

$$\phi = \beta l_o \tag{2}$$

where $\beta = (2\pi/\lambda)(n_x - n_y)$ is the propagation constant and n_x, n_y are the refractive indices of the principal axes, respectively. Therefore, if Δl is the elongation applied to the fiber, then the change in phase is

$$\Delta\phi = \beta\Delta l + l_o\Delta\beta \tag{3}$$

where $\Delta\phi$ = phase change due to external perturbations. The first term of eqn (3) represents the physical change of length produced by the strain. The second term, the change in ϕ due to

a change in β, results from two effects: the strain-optics effect whereby the strain changes the refractive index of the fiber, and a waveguide mode dispersion effect due to a change in fiber diameter, a, produced by longitudinal strain:

$$l_o\Delta\beta = l_o\left(\frac{d\beta}{dn}\right)\Delta n + l_o\left(\frac{d\beta}{da}\right)\Delta a \qquad (4)$$

where

$$\beta = \left(\frac{2\pi}{\lambda}\right)\Delta n = \left(\frac{2\pi}{\lambda}\right)B$$

λ is the wavelength of light propagating through the fiber, and $B = n_x - n_y$. The second term of eqn (4) can be dropped owing to the fact that it is very small compared with the first term. Thus eqn (3) becomes:

$$\frac{\Delta\phi}{\Delta l_o} = \left(\frac{2\pi}{\lambda}\right)\left[B + l_o\left(\frac{\Delta B}{\Delta l_o}\right)\right] \qquad (5)$$

Defining the axial strain as:

$$\epsilon = \Delta l/l_o \qquad (6)$$

and T_ϵ as the amount of strain required to produce a phase shift of 2π (one fringe), after omitting the intermediate steps, the change in phase due to strain can be expressed as:

$$\Delta\phi = \left(\frac{2\pi}{\lambda}\right)\left[B + \frac{\lambda}{T_\epsilon l_o^2}\right]\Delta l \qquad (7)$$

As per the definition for T_ϵ, $\Delta\phi/2\pi$ represents the number of fringes, N, that will be produced due to the change in length, Δl, and can expressed as:

$$N = \frac{\Delta\phi}{2\pi} = \left(\frac{B}{\lambda} + \frac{1}{T_\epsilon l_o^2}\right)\Delta l = \alpha\Delta l \qquad (8)$$

where

$$\alpha = \left(\frac{B}{\lambda} + \frac{1}{T_\epsilon l_o^2}\right)$$

Equation (8) provides the fundamental relationship between deformation and the number of fringes resulting from it. Since this relationship is linear, it is possible to develop a calibration constant relating the number of fringes to deformations.

CTOD SENSOR

Sensitivity of the fiber-optic sensor described in the preceding section is directly proportional to the gage length, l_o, of the Hi-Bi fiber.[7,5]. This can be explained by the Δl term in eqn (8). Other terms in eqn (8), i.e. λ and and B, are constants that depend on the wavelength of laser and the optical properties of the fiber. Compared with the effect of Δl, variations in the optical properties (λ and B) do not influence the number of fringes, N, in a significant manner. Since $\Delta l = \epsilon l_o$, for a number of optical fibers subjected to the same level of strain intensity, longer gage lengths (l_o) produce larger deformations. According to eqn (8), this will in turn increase the number of fringes, and therefore the resolving power of the sensor for the given strain level. Displacements associated with microcracking in concrete are of the order of a few μm. For typical values of $\lambda = 630$ nm, and $B = 0.00055$, this requires a sensing length, l_o, of about 0.5 m. As shown in Fig. 2(a), crack-

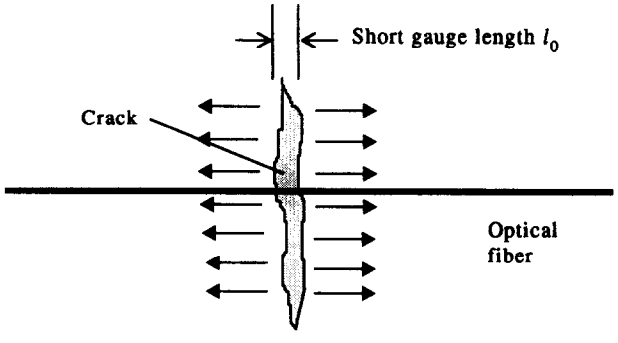

(a) Geometry of cracked and an embedded optical fiber in concrete

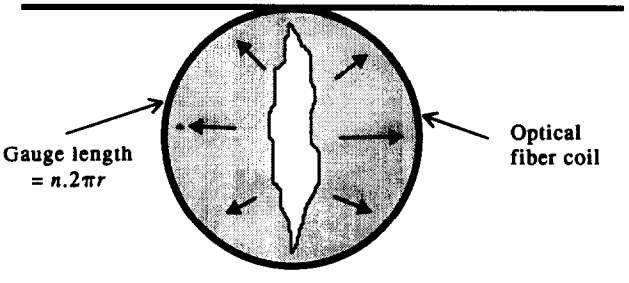

(b) Geometry of crack with respect to an optical fiber coil sensor

Fig. 2. Optical fiber and concrete cracks.

ing is a localized phenomenon, and deformations associated with microcracking in concrete specimens occur over a very short length of the optical fiber (a few mm). Therefore the Hi-Bi optical fiber, as described above, does not provide sufficient resolution for measurement of crack-tip opening displacements. However, it is possible to produce a very sensitive CTOD transducer by increasing the gage length of the optical fiber through the specific coil arrangement shown in Fig. 2(b). In this configuration, the optical-fiber coil is embedded in concrete on the plane perpendicular to the direction of crack-opening displacements at the notch tip. The gage length, l_o, is chosen by the circular bend diameter, and the number of loops in the coil. If n represents the number of loops in the coil, and r is the radius of the circular bend, then $l_o = n2\pi r$. Sensitivity of the transducer can be most efficiently increased by increasing the number of loops in the coil. This arrangement does not produce a bulky transducer, since optical fibers are extremely thin (typically 200 μm in diameter).

EXPERIMENTAL INVESTIGATION

The experimental program was designed for evaluation of the fiber-optic CTOD transducer. Experiments involved testing standard three-point bend center-edge-notched concrete beams. Typical beam dimensions and the geometry of embedded optical fiber with respect to the notch tip are given in Fig. 3. The determination of the number of loops, n, in the fiber-optic coil was based on experiments with three different sensors, each with a different n. A calibration procedure was developed in order to determine the calibration constant relating the number of fringes corresponding to a unit displacement.

Specimen preparation

The mix proportions by weight of the concrete used in this study were 1:1.1:2.0:0.35:0.10, corresponding to cement:sand:aggregate:water:silica fume. Type I Portland cement conforming to ASTM C 150, ASTM No. 2 grade river sand passing through sieve No. 8, and maximum coarse aggregate size passing 9.5 mm and retained on No. 4 sieve were used. Specimens were cast in Plexiglass molds. The coil optical-fiber sensor was placed at the tip of the notch (at approximately 2 mm above the notch tip) in the mold with the aid of six thin bars, 0.5 mm diameter, in a circular arrangement. Specimens were cured in a curing room for about 3 weeks before testing.

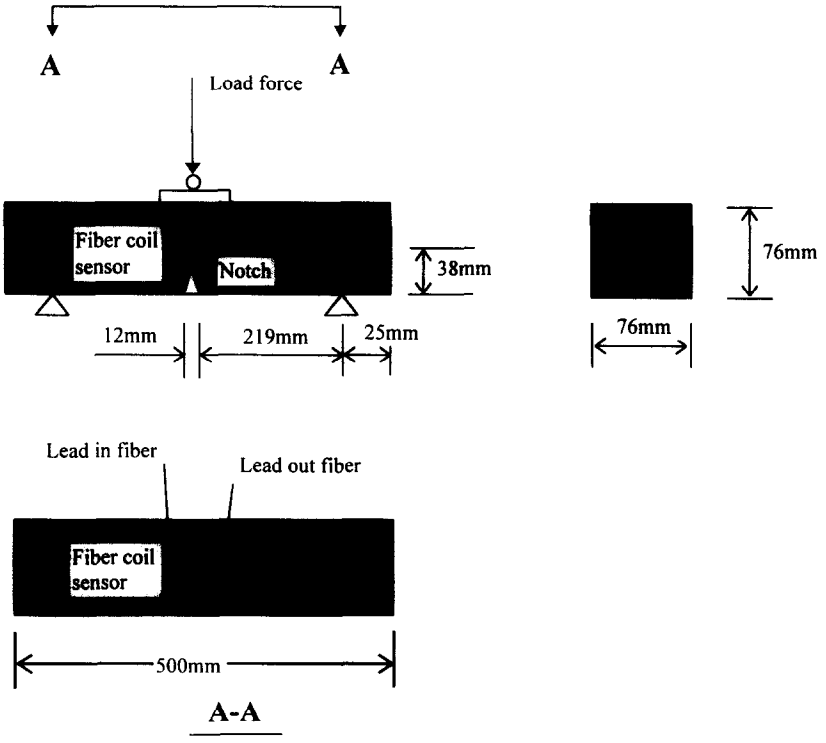

Fig. 3. Typical beam dimensions and location of embedded optical fiber in concrete.

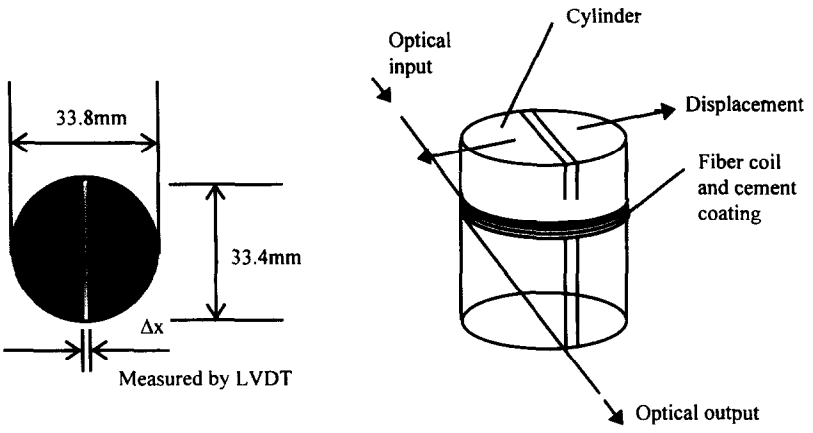

Fig. 4. Calibration set-up.

Calibration

Correlation between displacements and the corresponding fringes was accomplished by way of calibration. The calibration constant, α, as given in Fig. 8, was found from a plot of N vs Δl. The configuration shown in Fig. 4 corresponds to the calibration process, and for simplicity it does not include the laser and polarization optics. As shown in Fig. 4, the opening of the crack tip is simulated by the separation of cylinder halves. Crack-opening

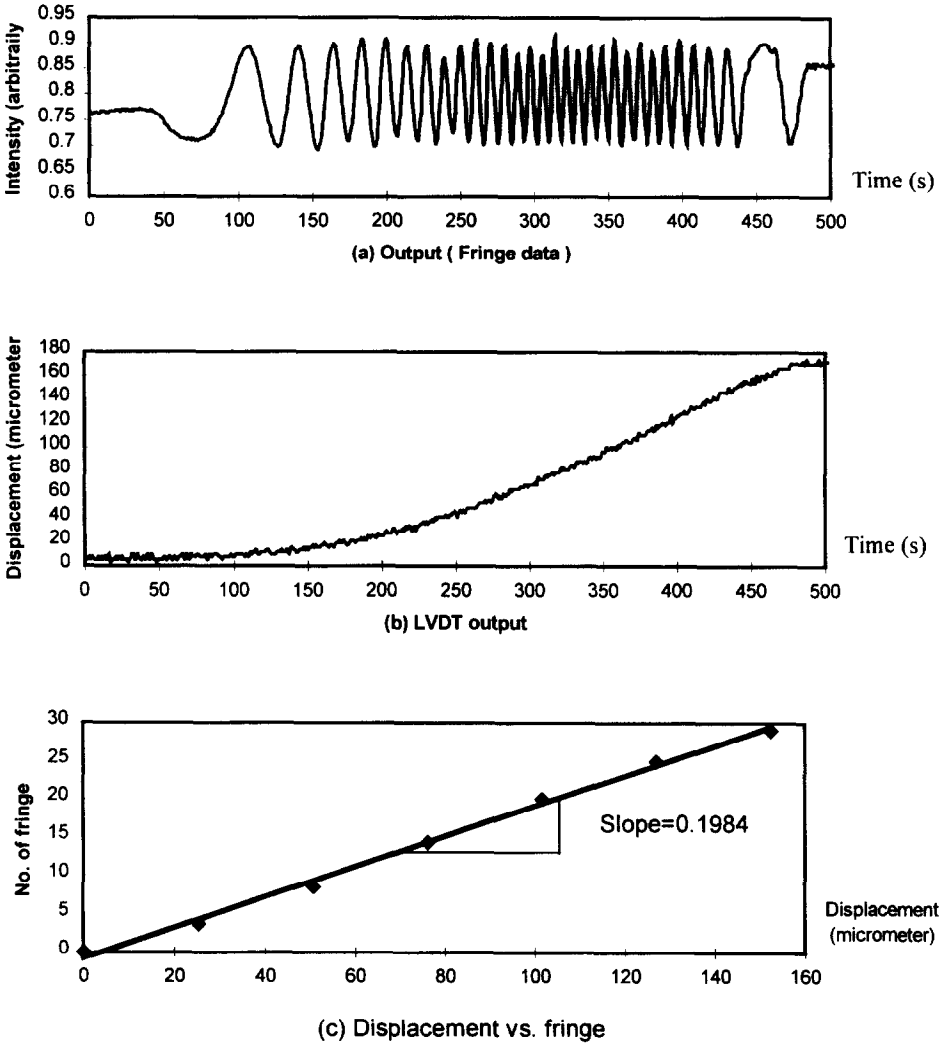

Fig. 5. Calibration results for fiber-optic coil with $n = 7$.

displacements along the crack profile in concrete are not uniform, mainly due to aggregate interlock. Therefore, the calibration similitude given in Fig. 4 corresponds to an average CTOD value along the crack profile.

The calibration process involves using Portland cement paste for fixing the fiber optics around two cylinder halves of diameter 33.8 mm. Polarization optics at the optical input and output will be explained in the following

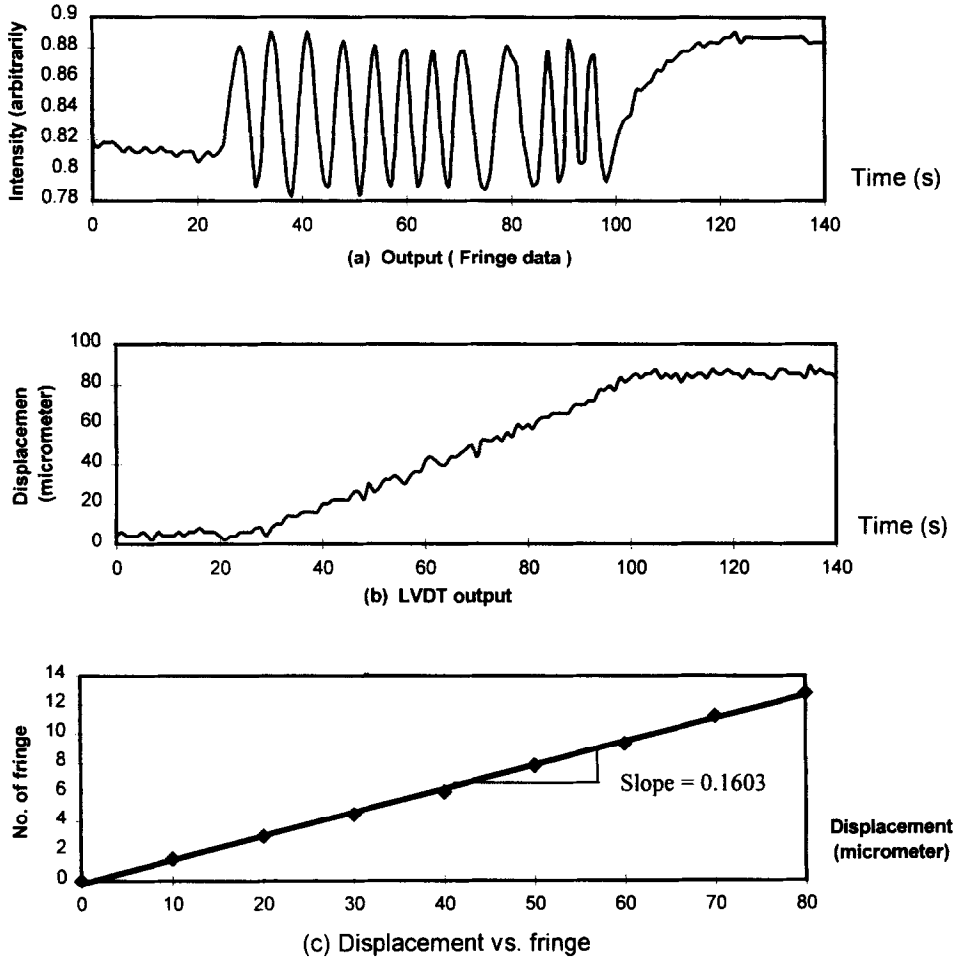

Fig. 6. Calibration results for fiber-optic coil with $n = 5$.

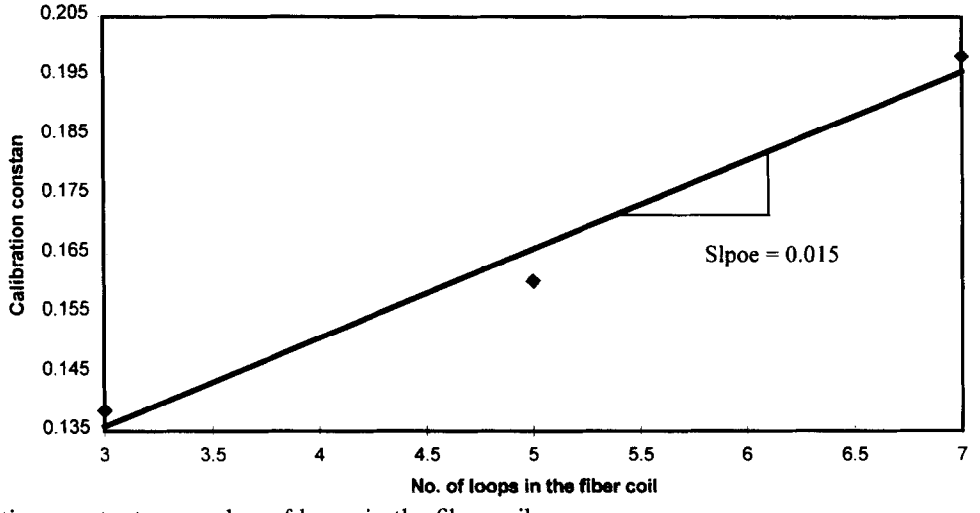

Fig. 7. Calibration constant vs number of loops in the fiber coil.

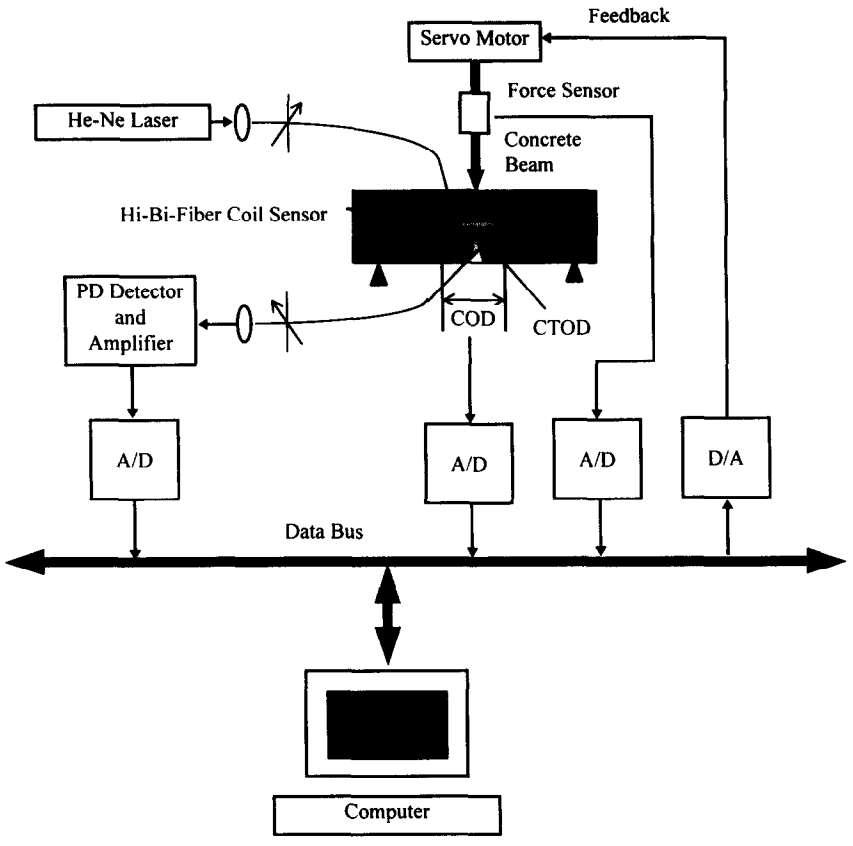

Fig. 8. Experimental set-up.

section. A motorized micrometer positioner separates the cylinder halves, and an LVDT measures the separation. The cement paste coating employed for affixing the optical fiber to the calibration cylinder prevents slippage and simulates bonding of the fiber in concrete. A data acquisition board was employed for receiving the optical fringe [Fig. 5(a)], as well as the data transmitted by the LVDT upon separation of the cylinder halves [Fig. 5(b)]. As shown in Fig. 5(c), the calibration constant, α, can be obtained by calculating the slope of the line relating the number of fringes to displacements. Data presented in Fig. 5 correspond to the fiber coil with 7 loops ($n = 7$). Figure 6 depicts calibration data for the fiber coil with 5 loops ($n = 5$). Another set of experiments were also performed with a fiber coil consisting of only 3 coils. The sensor with $n = 7$ provided sufficient sensitivity, and it was employed for embedment in concrete beams. As shown in Fig. 7, the sensitivity of the sensor (calibration constant) is directly related to the number of loops in the optical-fiber coil. The linear correlation

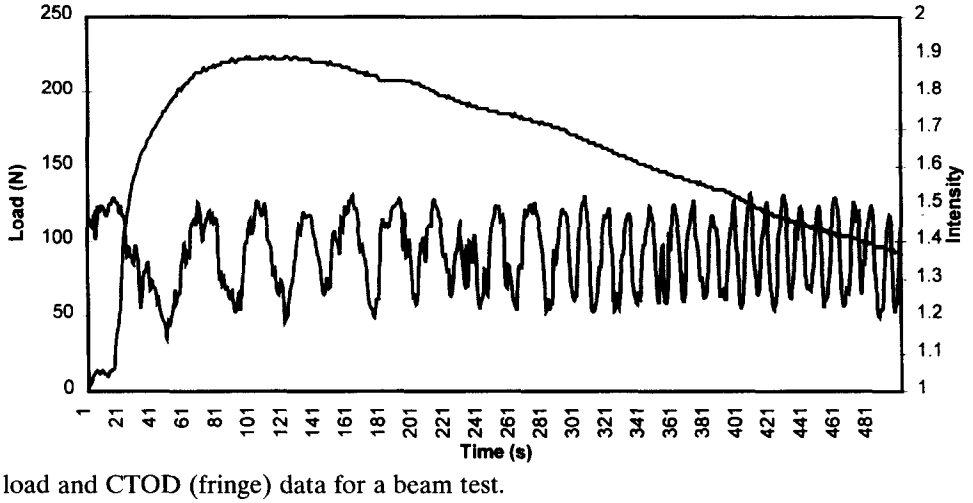

Fig. 9. Typical load and CTOD (fringe) data for a beam test.

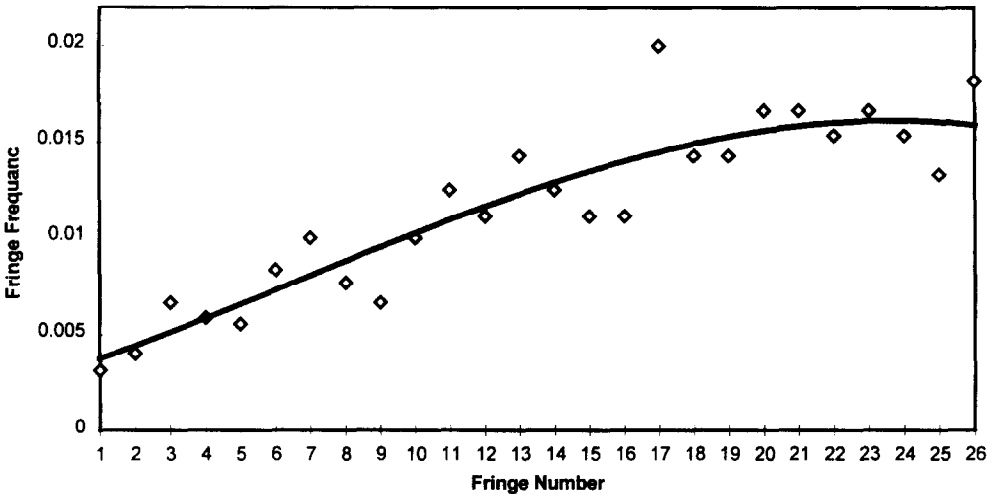

Fig. 10. Fringe number vs fringe frequency.

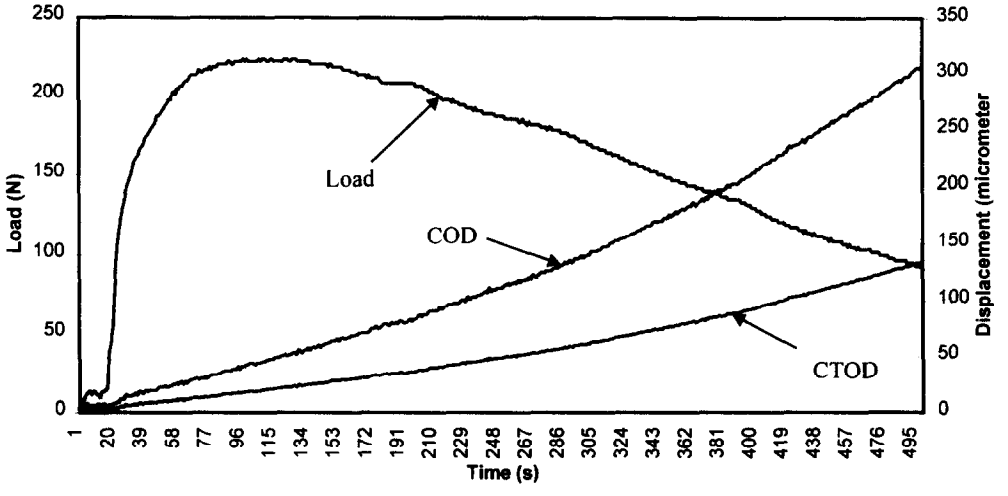

Fig. 11. Load, COD, and CTOD data for a typical concrete beam.

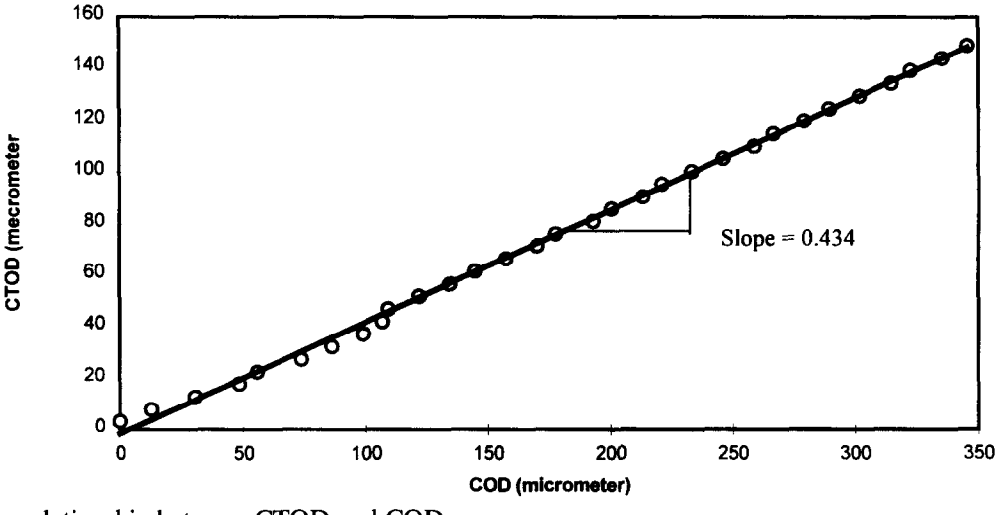

Fig. 12. Linear relationship between CTOD and COD.

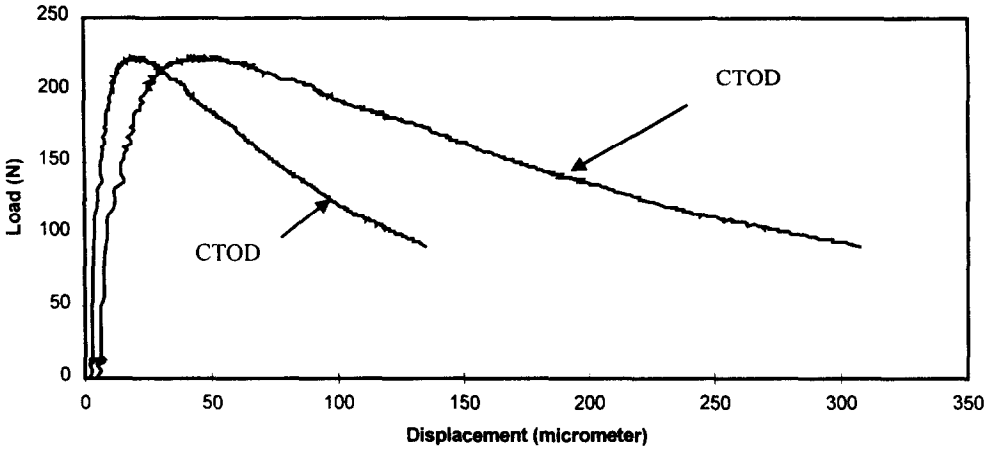

Fig. 13. COD and CTOD vs load.

depicted in Fig. 7 provides a useful tool for design of coil sensors.

Three-point bend tests

Three-point bend tests were performed in a closed-loop testing system under constant COD rate in order for the crack to grow in a controlled manner. COD was measured by an extensometer. CTOD was monitored by the fiber-optic sensor ($n = 7$). Four identical specimens were cast for experiments. The experimental configuration is shown in Fig. 8. The polarization optics include a polarized helium–neon laser, a lead-in fiber for delivery of light into the embedded Hi-Bi fiber at 45°, a lead-out fiber at 45°, a photo detector and amplifier assembly, and a multichannel data-acquistion system for transfer of data to the computer.

RESULTS AND DISCUSSIONS

Figure 9 depicts results obtained from a typical beam test. These results consist of the applied load, and the fiber-optics (CTOD) data in the form of optical fringes. The progressive increase in fringe frequency in Fig. 9 is indicative of an increase in CTOD rate during the cracking process. These data indicate that the CTOD rate does not increase in a linear manner, even though the three-point bend tests were performed in a closed-loop testing system under constant COD rate. Figure 10 is a plot of fringe frequency vs fringe numbers. It illustrates the increase in CTOD rate during crack propagation, and shows that the crack growth rate reaches a steady-state level which corresponds to the point half-way down in the descending branch of the load–time diagram. It is perceived that the half-way point in the descending branch of the load–time diagram corrresponds to the point where, at the tip, microcracks have coalesced into a macrocrack. If this is the case, then the visibility of the macrocrack which usually occurs at peak is only a surface phenomenon. Furthermore, the best-fit curve in Fig. 10 is asymptotic, indicating the steady-state crack growth level for the concrete beam.

Load, COD and CTOD data are plotted in Fig. 11. As shown in this figure, the relationships between the crack displacements (COD and CTOD) and time are non-linear. Yet, the plot of CTOD vs COD in Fig. 12 indicates that the relationship between the two displacements is linear, and it is possible to use this relationship in fracture models. In Fig. 13, load vs COD and CTOD data are plotted on the same graph for comparison. COD values are much larger than CTOD results mainly owing to the fact that they are obtained further away from the neutral axis (by 38 mm). Most fracture models have employed a critical COD value in their modeling. In these models CTOD values are determined through linear extrapolation of measured CODs. Relationships such as the one given in Fig. 12 can be employed to examine the validity of such models.

CONCLUSIONS

An optical-fiber sensor has been developed that can be embedded within cementitious composites for the measurement of crack-tip opening displacements. A calibration technique was

developed for conversion of optical data into the displacements associated with the opening of microcracks. Calibration results indicated that the sensitivity of measurements is directly dependent on the number of fiber loops within the sensor coil. By using the present coil geometry, experiments with concrete beams indicated displacement resolving powers as small as 5 μm. Fiber-optic data suggest that the crack-tip opening displacements are much smaller than the traditionally measured displacements at the crack mouth. The relationship between CTOD and COD was found to be linear. The frequency of optical fringes provided a new tool for measurement of crack growth rate. Fringe frequency data suggest that steady-state crack growth occurs after the peak load, and at loads half as large as the peak value.

ACKNOWLEDGEMENTS

This study was made possible by a grant from the National Science Foundation, grant number CMS-9402671, to the New Jersey Institute of Technology.

REFERENCES

1. Jenq, Y. S. & Shah, S. P., Nonlinear fracture parameters for cement based composites: theory and experiments. In *Proc. Applications of Fracture Mechanics to Cementitious Composites*. Martinus Nijhoff Publishers, Dordrecht, 1985, pp. 319–359.
2. Ansari, F., Mechanism of microcrack formation in concrete. *ACI Mater. J.*, **86**(5) (1989) 459–464.
3. Ansari, F., Stress/strain response of microcracked concrete in direct tension. *ACI Mater. J.*, **84**(6) (1987) 481–490.
4. Rashleigh, S. C., Polarimetric sensors: exploiting the axial stress in high birefringence fibers. In *Proc. Inst. Electr. Engrs, First Int. Conf. on Optical Fiber Sensors*, London, 1983, pp. 210–213.
5. Nanni, A., Yang, C. C., Kun, P., Wang, J. S. & Michael, R. R., Fiber-optic sensors for concrete strain/stress measurement. *ACI Mater. J.*, **88**(3) (1991) 257–264.
6. Ansari, F. & Wang, J., Rate sensitivity of high birefringent fiber optic sensors under large dynamic loads. *IEEE J. Lightwave Eng.*, **13**(10) (1995) 1992–1997.
7. Jackson, D. A., Monomode optical fiber interferometers for precision measurement. *J. Phys. E*, **18** (1985) 981–1001.